Article

Not peer-reviewed version

# Charge Resolution Study on AMS-02 Silicon Layer-0 Prototype

Alessio Ubaldi and Maura Graziani *

Posted Date: 10 November 2023

doi: 10.20944/preprints202311.0667.v1

Keywords: AMS-02 Layer 0 upgrade; Silicon micro-strips detector; nuclei; charge resolution; ADC

*Article*

# Charge Resolution Study on AMS-02 Silicon Layer-0 Prototype

**Alessio Ubaldi [1,2] and Maura Graziani [1,2,*]**

[1] Dipartimento di Fisica, Università degli Studi di Perugia, 06132 Perugia; alessio.ubaldi@studenti.unipg.it (A.U.); maura.graziani@unipg.it (M. G.)
[2] INFN Sezione di Perugia, Via Alessandro Pascoli, 23c, 06123 Perugia PG; alessio.ubaldi@pg.infn.it (A.U.); maura.graziani@pg.infn.it (M.G)
* Correspondence: maura.graziani@pg.infn.it

**Abstract:** The work presented in this paper represents a preliminary study on the performance of the new Silicon tracker layer, the Layer 0 (L0), that will be installed on top of the Alpha Magnetic Spectrometer (AMS-02), at the end of 2024. AMS-02 is a cosmic rays (CR) detector that has been operating on the International Space Stations (ISS) since May 2011. Thanks to its 9-layer Silicon tracker, this apparatus can perform high energy CR measurements with an unprecedented level of statistics and precision. However, high Z ($Z \geq 15$) CR nuclei statistic is strongly affected by fragmentation along the detector: with the installation of the new Silicon layer will be possible to achieve new unique high energy (TeV region) measures for those nuclei along with increased statistics for all nuclei up to Zinc. To achieve this, a Silicon ladder prototype, that will be part of the final Silicon layer, has been exposed to an ions test beam at the super-proton-synchrotron (SPS) of the CERN to characterize its charge resolution and the readout electronics. Preliminary results have shown a charge resolution of 10% for nuclei up to Z = 7.

**Keywords:** AMS-02 Layer 0 upgrade; Silicon micro-strips detector; nuclei; charge resolution; ADC

## 1. Introduction

By CRs we mean various species of energetic particles, charged or not, coming from space with galactic and extra-galactic origin. After the discovery of radioactivity (1896, A. H. Becquerel), it was observed that the rate of discharge of an electroscope increased considerably when it approached radioactive sources. Between 1901 and 1903 numerous researchers noticed that electroscopes discharged even when shielded, deducing that highly penetrating radiation contributed to the spontaneous discharge. The evidence of CRs extraterrestrial origin is mainly due to the Austrian-American physicist Victor Franz Hess and the Italian physicist Domenico Pacini in the early twentieth century. Hess discovered an increase of radiation intensity with altitude in 1912 [1] and was awarded the Nobel Prize in 1936 for that. As well as having established the foundation of particle physics, CRs discovery and study provided important contributions to understanding the physical processes underlying the astrophysics phenomenon and allowed to get closer to a complete and more detailed comprehension of fundamental mechanisms of particle physics.

CRs are divided in primary ones, that are produced by astrophysical sources, and secondary ones that are produced by the interactions of the primaries with the interstellar medium. At the top of Earth's atmosphere the CR radiation is composed of $\sim$ 90% of protons, $\sim$ 8% of Helium nuclei, $\sim$ 1% higher charge nuclei, and $\sim$ 1% of electrons, positrons, and antiprotons. Most CRs arriving at Earth' surface are constituted by muons that are a by-product of particle showers formed in the atmosphere by galactic CRs, starting from a single energetic particle. The study of CRs allows one to investigate a wide range of phenomena such as: production, acceleration and propagation of the latter. Nowadays, CRs and accelerators particle physics represent two complementary studies with the aim of solving the current physics mysteries such as the presence of dark matter or the absence of primordial anti-matter in our universe.

 doi:10.20944/preprints202311.0667.v1



CRs spectrum (number of particles per energy unit, time unit, surface unit and solid angle) is well described by a power law of the energy, with power index $\sim -2.7$ for primary nuclei up to $10^{15}$ eV. The most common way to describe the spectrum is by particles per rigidity R: the rigidity R, measured in volts, is defined as R=cp/q, where p and q are respectively the momentum and charge of the particle. Particles with different charges and masses have the same dynamics in a magnetic field if they have the same rigidity R.

The AMS-02 experiment is capable of performing precise and continuous measurements of CRs providing a large amount of statistics and data since its installation on the ISS in May 2011. The apparatus is composed of different subdetectors to measure the characteristics of traversing particles. The core of the instrument is formed by a Silicon tracker composed by nine layers of Silicon micro-strip sensors. A permanent magnet surrounds six layers, forming the spectrometer (inner tracker) that is able to measure the charge sign of a traversing particle. The Transition Radiation Detector (TRD), located at the top, identify and separate leptons ($e^{\pm}$) from hadrons ($p$ and nuclei). Time-of-flight systems (ToF) determine the direction and velocity of incoming particles and measure their charge. Anti Coincidence Counters (ACC), surrounding the tracker in the magnet bore, reject particles entering sideways. The Ring Imaging Cherenkov counter (RICH) provides a high precision measurement of the velocity. The Electromagnetic Calorimeter (ECAL) is a 3-dimensional calorimeter of 17 radiation lengths that provides energy measurements of positrons and electrons.

AMS-02 has the unique capability of distinguishing matter from antimatter, thanks to its capability of measuring the charge sign from the track deflection within its magnetic field. No other experiment currently taking data has a similar capability, nor is it foreseen to have one in the near future. In January 2020, AMS-02 was serviced with the installation of a new cooling system, Upgraded Tracker Thermal Pump System (UTTPS). In the new configuration, AMS is supposed to take data for the whole life of the ISS, that currently extends to 2030.

The latest report from the AMS collaboration [2] has highlighted an unprecedented observation: primary CRs have at least two distinct classes of rigidity dependence (Ne, Mg, Si and He, C, O). Moreover, it has been observed that the rigidity dependencies of primary and secondary CRs fluxes (Li, Be, B) are distinctly different. These results together with ongoing measurements of heavier elements in CRs will enable to determine how many classes of rigidity dependence exist in both primary and secondary CRs and provide important information for the development of the theoretical models.

Be able to measure nuclei charge and charge sign with high precision is a fundamental required to acquire significant amount of data and retrieve important information about CRs physics. In order to do that, an upgrade (Layer 0 upgrade) will be installed on top of the AMS-02 experiment. The AMS-02 Layer 0 upgrade consists of two planes of Silicon micro-strip sensors, both composed by 36 electromechanical units called "ladder". The upgrade will provide an increase of a factor 3 of the acceptance in many analysis channels, along with 2 new measurements of charge. Also, it will ensure access to a new region of high energy physics (TeV region) where no data actually exists. Elements from Z=15 to Z=30 have limited statistics: the upgrade will enable to perform complete and accurate measurements of the spectra of the elements up to Zn and will provide the foundation for a comprehensive theory of CRs. Moreover, the study of secondary CRs with Z>14 will provide complete and unique understanding of the CRs propagation charge dependence, which is of widespread interest in physics.

In order to achieve these goals, a complete and accurate characterization of the performances of the Silicon that will be installed on the apparatus is of fundamental importance. This preliminary work focuses on the study of one of those ladders that will be mounted on Layer 0 planes: in particularly, after a description of the components present in the detector, the process of analysis will be reviewed, starting from the calibration of the Silicon sensors and the electronics, going through the corrections applied to the signal and finally arriving to the evaluation of the actual charge resolution of the ladder.

Preprints (www.preprints.org) | NOT PEER-REVIEWED | Posted: 10 November 2023 doi:10.20944/preprints202311.0667.v1



## 2. Materials and Methods

The Layer 0 Silicon ladder prototype is a fundamental electromechanical unit composed of 10 Silicon sensors and an electronics front-end (LEF) board, which allows measurements of charge and position of a passing particle. The main characteristics of the used Silicon are reported on Table 1.

**Table 1.** Main characteristics of the ladder prototype and the Silicon sensors used.

| Parameter | Rating | Unit |
|---|---|---|
| Device type | Single side AC-readout | - |
| Silicon type | n-type Phosphorus doped | - |
| Crystal orientation | $< 100 >$ | - |
| Thickness | $320 \pm 15$ | $\mu$m |
| Front side metal | AL | - |
| Back side metal | AL | - |
| Chip size | $113\,000 \pm 20 \times 80\,000 \pm 20$ | $\mu$m |
| Active area | $111588.75 \times 78840$ | $\mu$m |
| Number of strips | 4096 | ch |
| Strip pitch | 27.25 | $\mu$m |
| Number of readout strips | 1024 | - |
| Readout strip pitch | 109 | $\mu$m |
| Strip width | 10 | $\mu$m |
| Readout AL width | 12 | $\mu$m |
| Readout PAD size | $56 \times 300$ | $\mu$m |

Sixteen application-specific integrated circuits (ASICs) located on the LEF, named IDE1140 or VA, read out 64 Silicon micro-strips each. Each ASIC includes an array of 64 spectrometric channels, an analog multiplexer (MUX), the registers and logic elements. An individual spectrometric channel contains a charge-sensitive pre-amplifier (PA), a shaping amplifier (Shaper) and a sample & hold unit. The sample & hold units are triggered by a common external signal (HOLD) which is generated by a field-programmable gate array (FPGA) after receiving an external trigger signal. While HOLD signal is high, the FPGA sends 64 clock pulses to the MUX, providing sequential readout of signal values held in the sample & hold units. Then the sampled signal is amplified in the VA. Finally, all signals are digitized by analog-to-digital converters (ADC).

An ions beam test was performed in November 2022 at the super-proton-synchrotron of the CERN: a 40 mm Beryllium target was hit by a primary beam of Pb (379 GV/c) which produced ions by fragmentation. The fragments were selected magnetically, in the rigidity interval of few % around 300 GV/c. At this scale of rigidity, every ion is considered a minimum ionizing particle (MIP).

The Bethe-Bloch formula describes the average energy loss by a particle with charge Z that traverses a target: for a fixed $\beta = \mathrm{v/c}$ and a fixed target, that quantity only depends on the charge square $Z^2$ of the incident particle. These average ionization losses are stochastic in nature and the Bethe-Bloch formula gives the mean value of these losses: the fluctuations around this value, in thin materials, are well described by the convolution of a Gaussian and a Landau (LanGauss) distribution [3]. Many ions with the same charge Z will generate such a convolution, from which the charge of the ion and the resolution of that charge can be derived. Having a beam with a population of different ions with different charges, the population distribution will be the sum of the single convolutions provided by the individual species.

### *2.1. Calibration and clusterization*

The ADC values of the readout strips for the $i$-th channel on the $j$-th VA pre-amplifier in the $k$-th event can be written as:

$$x_{ij}^k = p_{ij} + c_j^k + s_{ij}^k + q_{ij}^k \tag{1}$$

Preprints (www.preprints.org) | NOT PEER-REVIEWED | Posted: 10 November 2023 doi:10.20944/preprints202311.0667.v1



where $p_{ij}$ is a constant offset pedestal (unique for each channel), $c_j^k$ a coherent common noise component (that affects in the same way all the channels belonging to the same VA), $s_{ij}^k$ the strip noise and $q_{ij}^k$ an eventual signal due to the passage of a ionizing particle in the depleted Silicon. The calibration procedure consists in the determination of noise ($\sigma_s$) for each readout channel, recording $n$ events in absence of incident particles ($q_{ij}^k = 0$):

$$\sigma_s = \sqrt{\frac{1}{n}\sum_{k=1}^{n}(s_{ij}^k)^2} = \sqrt{\frac{1}{n}\sum_{k=1}^{n}(x_{ij}^k - c_j^k - p_{ij})^2} \tag{2}$$

To determine the noise is necessary to evaluate the pedestal $p$ and the common noise values $c$. The first half part of the $n$ taken events establishes the preliminary values of the strip pedestals ($p_{ij}^{RAW}$):

$$p_{ij}^{RAW} = \frac{2}{n}\sum_{k=1}^{n/2} x_{ij}^k \tag{3}$$

and its standard deviations:

$$\sigma_{ped}^{RAW} = \sqrt{\frac{2}{n}\sum_{k=1}^{n/2}(x_{ij}^k - p_{ij}^{RAW})^2} \tag{4}$$

The final values of strip pedestals are computed using the second half of the $n$ taken events using:

$$p_{ij} = \frac{2}{n}\sum_{k=n/2}^{n} x_{ij,good}^k \tag{5}$$

where the ADC values $x_{ij,good}^k$ are the ones inside $\pm 3\sigma_{ped}^{RAW}$ respect to $p_{ij}^{RAW}$. Thanks to this procedure, the too noisy channels for a given event, are excluded from the evaluation of the pedestals. The common noise is produced by the fluctuations of the power supply and other electromagnetic interferences, and it is constant for all the preamplifiers contained in the same VA. It is evaluated event by event for each VA, calculating the median value after subtracting the pedestal. This procedure defines a valid signal by applying a threshold to the signal-to-noise ratio (S/N) of the strip:

$$\frac{S}{N} = \frac{x_{ij}^k - c_j^k - p_{ij}}{\sigma_s} \tag{6}$$

After the calibration procedure, every channel signal contains two contributes: the strip noise and a possible value due to the crossing particle.

To correctly measure the charge of a crossing particle is needed to identify all the strips that are interested in collecting all the signal released in the Silicon by that particle or, in other words, is necessary to build a cluster. A cluster is a group formed by all the strips involved in the collection of the ionization energy loss by a particle. This process, called clusterization, is done by checking at the S/N of every readout strips: the first strip found with this ratio above a certain threshold ($n_H$) is defined as the seed of the cluster. All adjacent strips to the seed are added to the cluster until their S/N ratio is above a second lower threshold ($n_L$). This procedure is done for all the 1024 readout strips of the Silicon ladder. An example is reported in Figure 1.

Preprints (www.preprints.org) | NOT PEER-REVIEWED | Posted: 10 November 2023 doi:10.20944/preprints202311.0667.v1



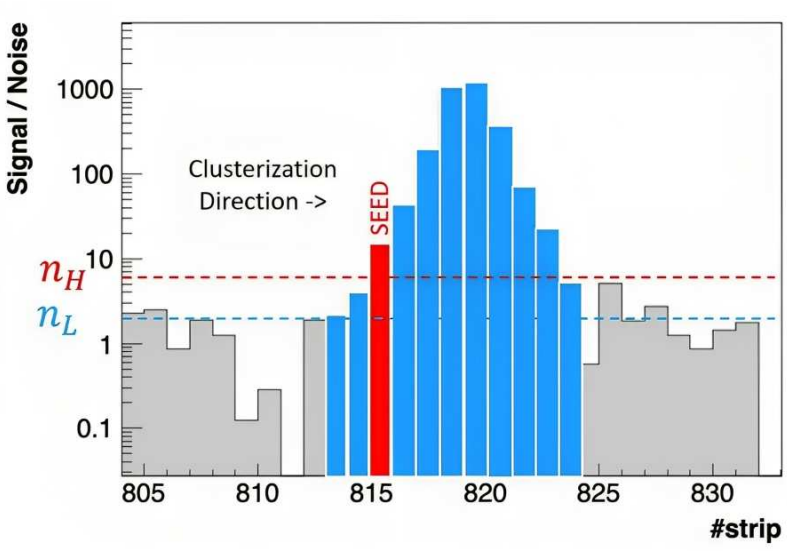


**Figure 1.** Signal over noise ratio (in logarithmic scale) as a function of the strip number for a single event. The red line indicates the higher threshold $n_H$ that defines the cluster seed. All adjacent strips to the seed are added to the cluster until their S/N ratio is above the blue lower threshold $n_L$. The cluster will be formed by all the highlighted strips.

### *2.2. Trigger-to-hold time*

The time, or delay, between the arrival of the external trigger and the sampling of the signal is the so called trigger-to-hold time: waiting the correct amount of time between this two event is a crucial point in order to sample the peak time of the shaped signal. In order to find the best value for the trigger-to-hold time, a dedicated study on CERN beam test data was performed. During the data acquisition, different runs with about the same amount of data have been taken with different values of trigger-to-hold time. In total, 6 data set with respectively 3.5 $\mu$s, 5.5 $\mu$s, 6.5 $\mu$s, 7.5 $\mu$s, 8.5 $\mu$s and 9.5 $\mu$s of trigger-to-hold time have been analyzed. For each data set the distribution of the total cluster amplitude (ADC), where the amplitude is the sum of all contributes of all the individual cluster strips, was fitted using a Landau function. The behavior of the most probable values extrapolated from the fits as a function of the trigger-to-hold time is shown in Figure 2.

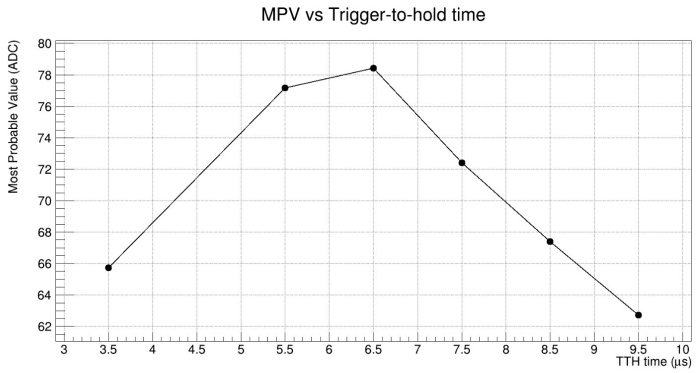


**Figure 2.** Most probable values as a function of the trigger-to-hold time. The value that allows the sample of the peak time is around 6.5 $\mu$s.

### *2.3. Eta correction*

Once all the events are clusterized it is possible to proceed with the evaluation of the charge resolution. The data-set used for the evaluation of the charge resolution was acquired with high and low clusterization thresholds of 5.5 and 2.0 respectively and with a trigger-to-hold time of $\sim$ 6 $\mu$s.

Preprints (www.preprints.org) | NOT PEER-REVIEWED | Posted: 10 November 2023 doi:10.20944/preprints202311.0667.v1



Selecting the most energetic cluster per event, i.e. the cluster with maximum amplitude, allows a noise rejection and good cluster choosing. The considered ladder has a total of 4096 Silicon micro-strips but only one every four adjacent strips (1024) is effectively read out by the electronics: the intermediates, called floating strips, are capacitively coupled to the readout ones and all the strips are also capacitively coupled to the metallized back plane allowing operation of the Silicon in overdepleted mode [4]. This electrical scheme leads to an inter-strip energy loss; when collecting ionization, the floating strips share all the acquired signal to the nearest readout strips, but when doing this, part of the signal is loss due to the capacitively coupled to the back plane. In first approximation, studying the signal shared between the two nearest strips to the particle impact position allows quantifying the inter-strips energy loss. A more realistic description of the capacitive charge sharing has to take in account not only the direct inter-strip capacitance to the first neighboring strips but also indirect coupling to the second and even third readouts [5]. The inter-strips energy loss is quantified by $\eta$, defined as follows:

$$\eta = \frac{S_1}{S_1 + S_2} \quad \eta \in (0,1) \tag{7}$$

where $S_1$ and $S_2$ are the signals in ADC of the two highest strips of the cluster (coinciding with the two nearest to the impact position). The dependency of the total cluster amplitude by eta is shown in Figure 3: the region between the two black lines corresponds to the energy deposited by Z=2 particles. To different eta values, i.e. different impact position with respect to the two highest strips of the cluster, correspond different ADC values for the same charge. To take into account this dependency, the ADC distribution has been supposed to be parabolic in eta and constant for every amplitude:

$$f(\eta) = a\eta^2 + b\eta + c \tag{8}$$

To find the coefficients of the parabola has been used the Z=2 sample. Has been fitted the cluster amplitude distribution, with a Landau function around the maximum, for three different eta intervals: $\eta \in \{[0, 0.08], [0.46, 0.54], [0.92, 1]\}$. The regions chosen for that purpose are shown in Figure 4 and the fits on Z=2 peak for the different regions are shown in Figure 5. The passage of the parable was imposed on three points, each one composed by the eta values (0,0.5,1) and the most probable values shown in Figure 5. The eta correction is finally defined as:

$$\omega = \frac{c}{f(\eta)} \tag{9}$$

To take rid of the inter-strip energy loss, every ADC value has been multiplied by $\omega = c/f(\eta)$, where $c$ is the known term of the parabola and $f(\eta)$ will be the parabola value at the eta point corresponding to the ADC value wanted to correct.

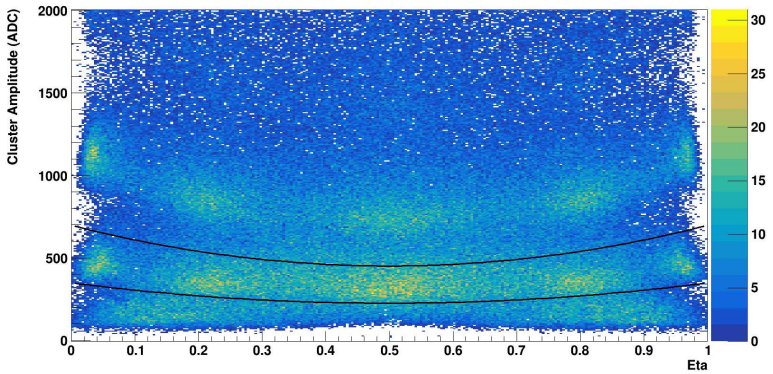


**Figure 3.** Cluster amplitude distribution as a function of eta. The region between the two black lines is the sample corresponding to $Z = 2$ chosen to characterize the eta dependency.

Preprints (www.preprints.org) | NOT PEER-REVIEWED | Posted: 10 November 2023 doi:10.20944/preprints202311.0667.v1



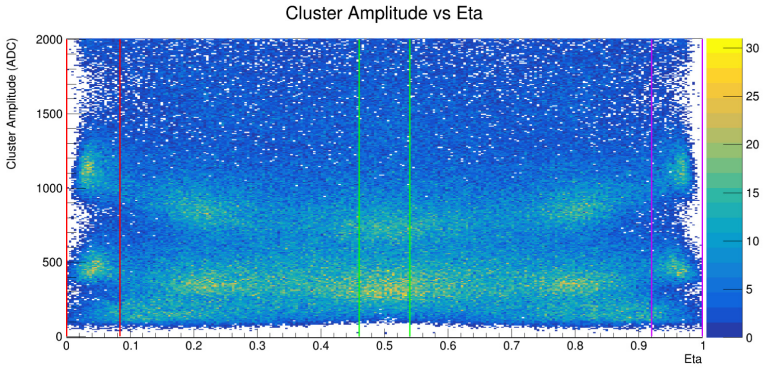


**Figure 4.** Cluster amplitude as a function of eta. In red, green and purple are highlighted the three selected eta intervals.

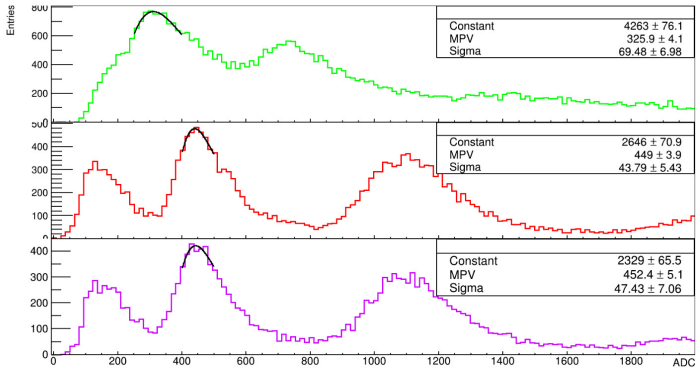


**Figure 5.** Distribution of the cluster amplitude for the three selected eta intervals: green (0.46÷0.54), red (0÷0.08) and purple (0.92÷ 1). The black lines represent the Landau fit around the maximum.

### *2.4. Va equalization*

Another signal correction has been doing considering the VAs: ideally one wants to observe the same response, i.e. the same ADC value, for each VA for a given Z. This doesn't happen and different VAs have different response functions that provide different ADC values for the same charges. An equalization of 9 of the 16 VAs (from number 5 to 13) was made, considering VA number 10 as a reference.

Figure 6 shows the corrected cluster amplitude distribution as a function of the strip number: in red label is highlighted the VA number, going from 1 to 16. To equalize the VAs with respect to VA number 10 has been studied the corrected cluster amplitude distribution inside a 64-channel range (that corresponds to a full VA). As mentioned, the distribution of a population containing different ions will be the sum of the single convolutions (between a Gaussian and a Landau) provided by each ion. Figure 7 reports the corrected cluster amplitude distribution for the VA number 10: the red lines represent the fit performed around the peaks with the convolution between a Gaussian and a Landau in order to estimate the most probable values for the energy deposited by charge from Z=2 to Z=7. The first peak corresponds to Z=1: despite is performed, Z=1 is excluded from the analysis.

The same procedure has been applied for the remaining 8 VAs. For the k-th VA (for a total of 9 VAs from number 5 to 13), the fits give six most probable values $MPV_i^k$, with i=2,.. ,7 and k=5,.. ,13. Then the response functions of every VA with respect to VA 10 have been built by doing the ratio between the most probable values of VA 10 ($MPV_i^{10}$) and the most probable values of the remaining VAs ($MPV_i^k$) as a function of $MPV_i^k$, $k \in \{5, 6, 7, 8, 9, 11, 12, 13\}$. For clarify, Figure 8 shows the ratio between VA number 10 and VA number 11.

Preprints (www.preprints.org) | NOT PEER-REVIEWED | Posted: 10 November 2023 doi:10.20944/preprints202311.0667.v1



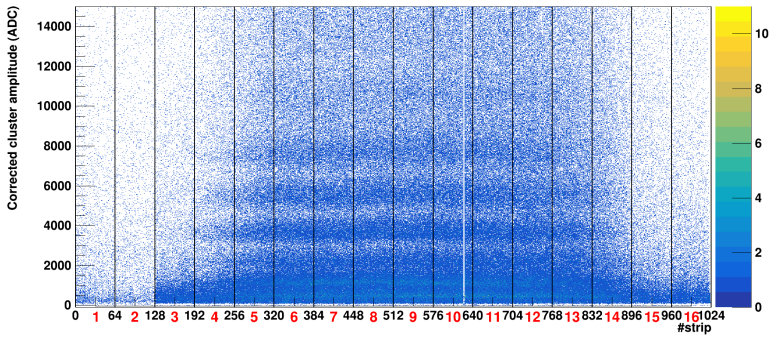


**Figure 6.** Corrected cluster amplitude distribution as a function of strip number. In red label is reported the VA number.

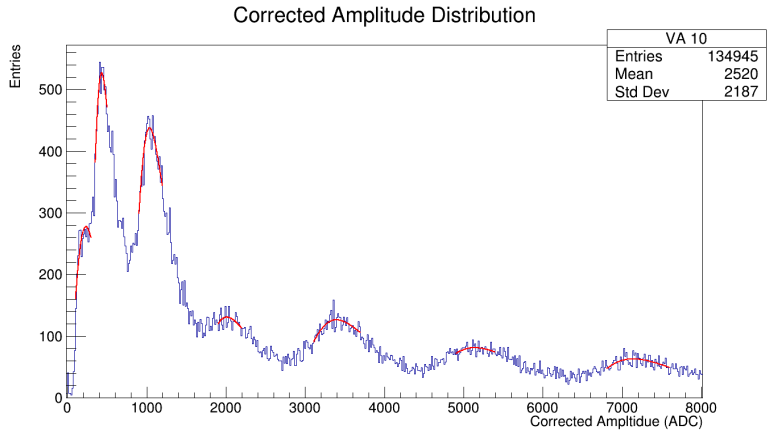


**Figure 7.** Corrected cluster amplitude distribution for the VA number 10. The red lines are the fit performed with the convolution of a Gaussian and a Landau around the peaks. The first peak corresponds to Z=1 but is excluded from the analysis.

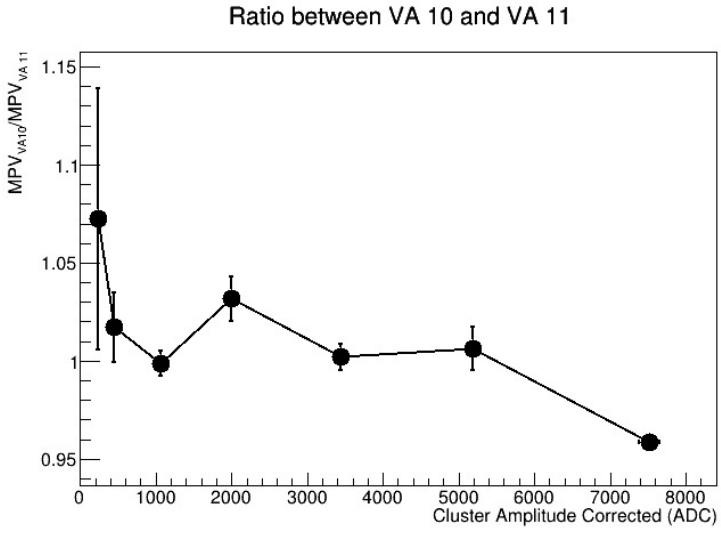


**Figure 8.** VA 11 equalization function (with respect to VA number 10). On the x-axis there is the corrected cluster amplitude for VA number 11 and on the y-axis there is the ratio between the most probable values of VA number 10 and VA number 11. Despite is reported, Z=1 is excluded from the analysis.

Preprints (www.preprints.org) | NOT PEER-REVIEWED | Posted: 10 November 2023 doi:10.20944/preprints202311.0667.v1



The first point correspond to Z=1: despite is reported, Z=1 is excluded from the analysis because the trigger conditions were set in order to minimize the acquisition of that type of event. So the statistics for Z=1 is very poor and inappropriate to perform any type of statistical analysis. In reference to the same figure, the poly line that joins the points represents the function used for the equalization of the VA number 11, $f^{11}$. The signal measured by the k-th VA, $S^k$, is equalized with respect to VA number 10 by:

$$f^k(S^k) \cdot S^k \tag{10}$$

where $f^k$ is the equalization function for the k-th VA, obtained with the same procedure explained for k=11.

### 2.5. Saturation

The analysis performed on the Silicon ladder was done up to Z=7 and was not possible to acquire higher charges because of electronics saturation. This behavior is due to the dynamic range of the VA and the pre-amplifier. Figure 9 shows the output of the VA as a function of the input signal. The VA output is a linear function of the input signal only below a certain value, that is 172 fC. As long as the input charge is below 172 fC, the VA output is linear with the charge, but above this threshold the VA gain decreases rapidly, leading to the same output for a large range of input charges. Incident particles generate an amount of ionization, and so a VA input, that is increasing with $Z^2$: the non-linear behavior of the VA for high charges has limited the analysis only to those charges with $Z \leq 7$.

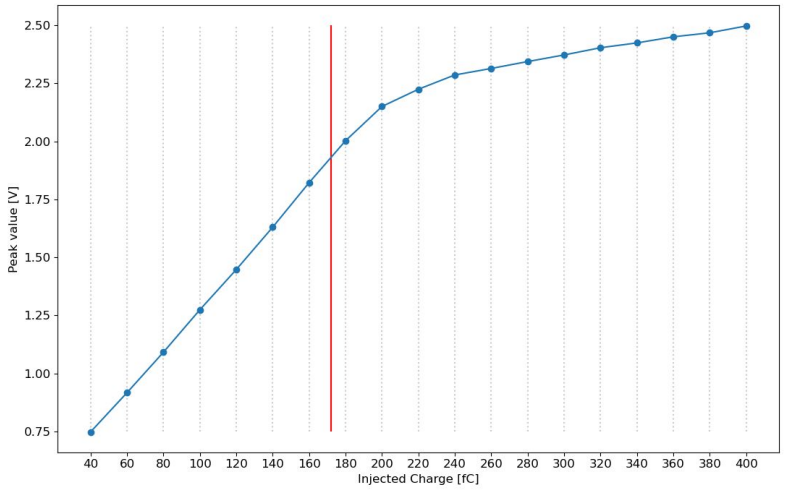


**Figure 9.** Voltage output of the VA as a function of the injected charge: the red line represents the declared limit of the linear range of the VA that corresponds to 172 fC.

### 2.6. Charge resolution

Figure 10 shows the distribution of the total cluster amplitude corrected by eta and equalized with respect to VA number 10 and the six convolution functions used to fit that distribution. The applied procedure to measure the final charge resolution is the following:

- The total cluster amplitude corrected by eta and equalized with respect to VA number 10 is fitted with six different LanGauss functions;
- The parameters obtained from the fits are used to generate a Monte Carlo (MC) toy for each charge sample by doing the square root o f a random event generated using the probability density functions (PDFs). Thanks to the Bethe-Bloch formula, the mean energy loss by a particle is proportional to $Z^2$ which is measured by the detector in ADC counts. In order to evaluate Z is needed to study the $\sqrt{ADC}$ distribution;

Preprints (www.preprints.org) | NOT PEER-REVIEWED | Posted: 10 November 2023 doi:10.20944/preprints202311.0667.v1



- The MC toy is used to apply the central limit theorem (CLT) to estimate the charge resolution.

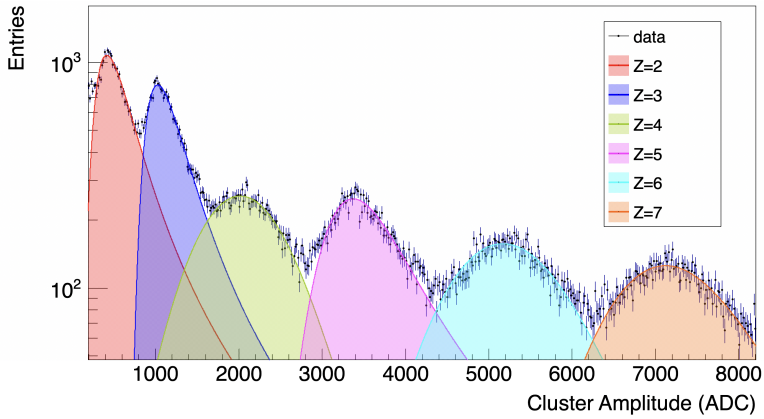


**Figure 10.** Distribution of the total cluster amplitude corrected by eta and equalized with respect to VA number 10. Every peak has been fitted using the convolution of a Gaussian and a Landau.

The PDFs $f_i(Z^2)$ with i = 2, ..,7, has been built. A sample of N=1000 events for the i-th charge has been generated by doing the square root of a random event created using $f_i(Z^2)$.

As example in Figure 11a is reported the $\sqrt{ADC}$ distribution for Z=3 and its arithmetic mean generated with the MC toy. The $\sqrt{ADC}$ distribution reported in the same figure follows a PDF, $f(Z)$, with an expectation value of $\hat{z}$ and variance $(\Delta z)^2$. The resolution of the charge will be $\Delta z/\hat{z}$.

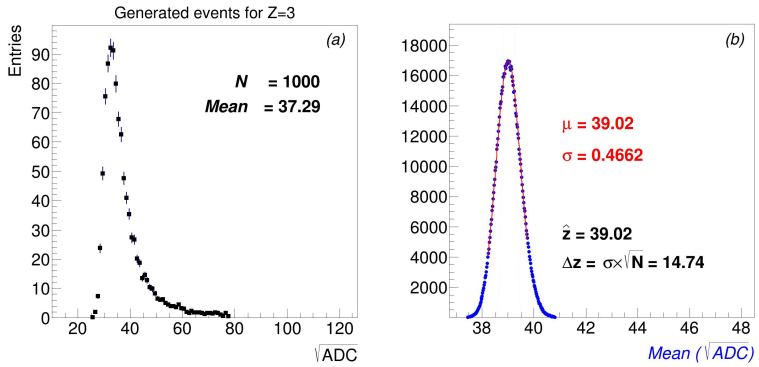


**Figure 11. (a)** Sample of N=1000 events containing the distribution of $\sqrt{ADC}$ generated with a Monte Carlo experiment with $f_3(Z^2)$ for Z=3. **(b)** Distribution of the mean $(\sqrt{ADC})$ for M=$10^6$ Monte Carlo experiments (each one with N=1000 events) for Z=3. According to the central limit theorem, is possible to evaluate $\hat{z}$ and $\Delta z$.

According to the central limit theorem (CLT), for a variable x with expectation value E[x] = $\hat{z}$ and variance V[x] = $(\Delta z)^2$, the distribution of the mean is Gaussian with mean $\mu$ and variance $\sigma^2$ linked to $\hat{z}$ and $(\Delta z)^2$ by:

$$\mu = \hat{z} \qquad \sigma = \frac{\Delta z}{\sqrt{N}}, \quad N \to \infty \tag{11}$$

Figure 11b shows the mean distribution for Z=3 for M=$10^6$ Monte Carlo experiments (each one with N=1000 events): is possible to evaluate $\hat{z}$ as the mean of the Gaussian distribution and $\Delta z$ as $\sigma \cdot \sqrt{N}$. Figure 12 shows the distributions of the means for all the charges under studying (from Z=2 to Z=7) and the relative Gaussian fit with mean $\mu$ and standard deviation $\sigma$.

Preprints (www.preprints.org) | NOT PEER-REVIEWED | Posted: 10 November 2023 doi:10.20944/preprints202311.0667.v1



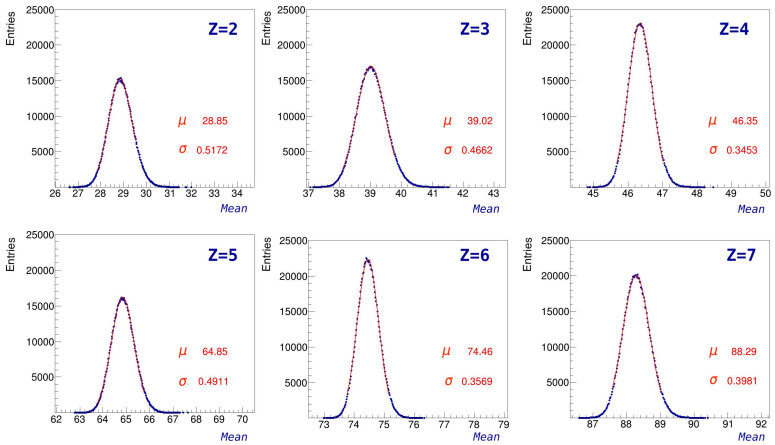


**Figure 12.** Distributions of the means for all the charges under studying (from Z=2 to Z=7) and the relative Gaussian fits with mean $\mu$ and standard deviation $\sigma$.

## 3. Results

### *3.1. Charge resolution*

Figure 13 shows the preliminary results we obtained for the charge resolution of the Layer 0 prototype for a single layer (red points) and for two layers (square blue points) compared with the charge resolution of the AMS-02 inner tracker (L2 to L8, hollow orange points). The Layer 0 upgrade will be composed by two planes and its overall charge resolution can be evaluated by the combination of two independent measurements. We evaluated the resolutions for two layers assuming that the charge resolution is the same for both: in this case is $1/\sqrt{2}$ times the resolution of a single layer. In Table 2 are reported the charge resolution values we evaluated for charges from Z=2 to Z=7 for a single layer of Layer 0 and for two layers. For comparison is also reported the values of the inner tracker (L2 to L8) charge resolution for the same charges.

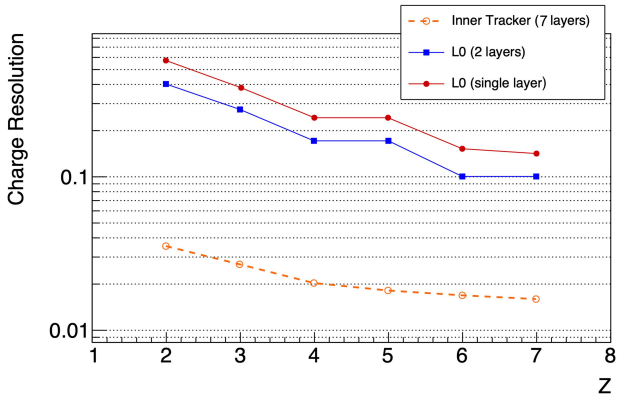


**Figure 13.** Preliminary charge resolution values as a function of charge Z we obtained for a single layer (red points) and for two layers (square blue points) of Layer 0 compared with the current charge resolution of the AMS-02 inner tracker, from Layer 2 (L2) to Layer 8 (L8) [6] (hollow orange points) that is obtained by the combination of 7 layers.

Preprints (www.preprints.org) | NOT PEER-REVIEWED | Posted: 10 November 2023 doi:10.20944/preprints202311.0667.v1



**Table 2.** Values of charge resolution we obtained for different Z values (first column) both for single layer (second column) and two layers (third column) of Layer 0. In the fourth column is reported the current AMS-02 inner tracker (L2 to L8) charge resolution.

| Z | L0 (single layer) | L0 (two layer) | Inner tracker (L2 to L8) |
|---|---|---|---|
| 2 | 0.57 | 0.40 | 0.035 |
| 3 | 0.38 | 0.27 | 0.027 |
| 4 | 0.24 | 0.17 | 0.02 |
| 5 | 0.24 | 0.17 | 0.018 |
| 6 | 0.15 | 0.10 | 0.017 |
| 7 | 0.14 | 0.10 | 0.016 |

To conclude, in Figure 14 is reported the comparison between the charge resolution we evaluated for a single layer of L0 with the charge resolution for a single layer of the AMS-02 inner tracker (L2 to L8).

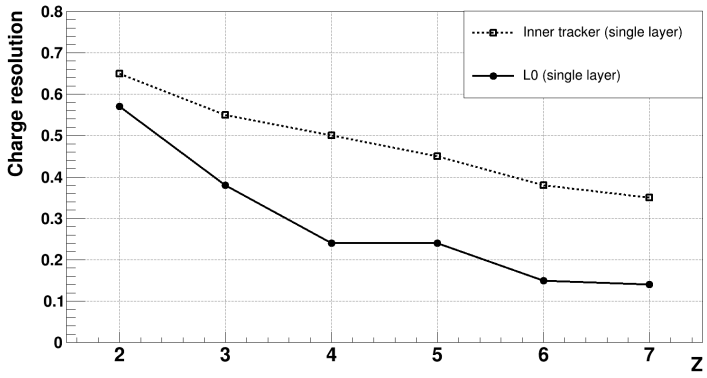


**Figure 14.** Charge resolution we evaluated for a single layer of Layer 0 (filled circles) compared with the charge resolution of a single layer of the AMS-02 inner tracker (L2 to L8, hollow squares) [6].

## 4. Discussion

The study performed on the Silicon AMS-02 Layer 0 prototype has shown agreement in therms of charge resolution with respect to the AMS-02 inner tracker. The signal collected by Silicon sensors has been analyzed after the calibration to find an algorithm that allows to discriminate the signal from the noise. After the selection of the signal, an accurate characterization of the signal released by the ion species has been performed with $2 \leq Z \leq 7$ in the Silicon sensors that will be used for the construction of layer 0. At the current state, the new layer on top of AMS-02 will be able to measure the charge at least up to Z=7 with a resolution of 10%.

The obtained resolutions can be further improved. For example, the lack of statistics for Z = 1, due to trigger conditions, can be compensated by future data acquired with a suitable setup to maximize the Z = 1 particles acquisition.

Furthermore, the applied correction for $\eta$ can be improved considering the different dependencies for different charges.

More, the saturation of the electronics (VA) has limited the acquisition of high charges to Z=7. Indeed, considering that the analog to digital converter has an input range of $0 \div 4$ V (full scale equals to $2^{14} - 1$ ADC = 16 383 ADC), is consistent with the fact that saturation appears at a VA output value of 2 V that corresponds approximately to 8000 ADC. By investigating the dynamic range of the VA itself and by studying the various amplify stages, it will be possible to study even higher charges.

Moreover, another improvements would be possible considering the fits performed on the cluster distribution of Figure 10: at the current state every contribution has been fitted with a single LanGauss function described by 5 parameters, for a total of six different LanGauss. The fit could be improved by using a single function constituted by the sum of six LanGauss that could possibly be more accurate.

 doi:10.20944/preprints202311.0667.v1



## 5. Conclusions

The work presented in this manuscript is the first preliminary characterization of the performance, in therms of charge resolution, of the new Silicon sensors that will be mounted on the AMS-02 Layer 0 upgrade.

The values we evaluated for the charge resolution for charges from Z=2 to Z=7 for L0 differ by an order of magnitude with respect to the current overall resolution of the AMS-02 inner tracker: this is due to the fact that the latter values are obtained by the combination of 7 layers.

Despite this, the values we evaluated for the charge resolution for single layer of Layer 0 are significantly smaller (2.5 times for Z=7) than the values for single layer of the AMS-02 inner tracker, as shown in Figure 14: this is promising, although the signal correction can be further improved. This will be a starting point for a future analysis and a complete characterization of the final Layer 0 charge resolution.

**Institutional Review Board Statement:** Not applicable.

**Informed Consent Statement:** Not applicable.

**Data Availability Statement:** The data presented in this study can be made available on request from the corresponding author.

**Conflicts of Interest:** The authors declare no conflict of interest.

## Abbreviations

The following abbreviations are used in this manuscript:

| | |
|---|---|
| L0 | Layer 0 |
| AMS | Alpha Magnetic Spectrometer |
| ISS | International Space Station |
| CR | Cosmic Ray |
| eV | electronvolt |
| TeV | Teraelectronvolt |
| SPS | super-proton-synchrotron |
| TRD | Transition Radiation Detector |
| ToF | Time of Flight |
| ACC | Anti Coincidence Counter |
| RICH | Ring Imaging Cherenkov |
| ECAL | Electromagnetic Calorimeter |
| UTTPS | Upgraded Tracker Thermal Pump System |
| LEF | L0 electronics front-end |
| ASIC | application-specific integrated circuit |
| MUX | analog multiplexer |
| PA | pre-amplifier |
| FPGA | field-programmable gate array |
| ADC | analog-to-digital converter |
| MIP | minimum ionizing particle |
| LanGauss | convolution of a Gaussian and a Landau |
| S/N | signal-to-noise ratio |
| MPV | most probable value |
| fC | femtoCoulomb |
| MC | Monte Carlo |
| PDF | probability density function |
| CLT | Central Limit Theorem |
| L2 | Layer 2 |
| L8 | Layer 8 |

## References

1. Hess, V. F. Über Beobachtungen der durchdringenden Strahlung bei sieben Freiballonfahrten *Phys. Z.* **1912**, *13*, 1084-1091
2. Aguilar, M.; Cavasonza, L. A.; Ambrosi, G. et al. The Alpha Magnetic Spectrometer (AMS) on the international space station: Part II — Results from the first seven years. *Phys. Rep.* **2021**, *894*, 1-116

 doi:10.20944/preprints202311.0667.v1



3. Hancock, S. et al. Energy loss and energy straggling of protons and pions in the momentum range 0.7 to 115 GeV/c. *Phys. Rev. A* **1983**, *28*, 615.
4. Lutz, G.; Schwarz, A. S. Silicon Devices for Charged-Particle Track and Vertex Detection. *Annu. Rev. Nucl. Part. Sci.* **1995**, *45*, 295–335
5. Dabrowski, W. et al. Study of spatial resolution and efficiency of silicon strip detectors with charge division readout. *Nucl. Instrum. Methods Phys. Res. Sect. A Accel. Spectrom. Detect. Assoc. Equip.* **1996**, *383*, 137–143
6. Jia, Y. et al. Nuclei charge measurement by the Alpha Magnetic Spectrometer silicon tracker. *Nucl. Instrum. Methods Phys. Res. Sect. A Accel. Spectrom. Detect. Assoc. Equip.* **2020**, *972*, 164169.